# On Exploiting Active Redundancy of a Modular Multilevel Converter to Balance Reliability and Operational Flexibility

Jaesik Kang, *Member, IEEE*, Heejin Kim, *Member, IEEE*, Hong-Ju Jung, *Senior Member, IEEE*, Dong-Su Lee, *Member, IEEE*, Chan-Ki Kim, *Senior Member, IEEE*, H. Alan Mantooth, *Fellow, IEEE*, and Kyeon Hur, *Senior Member, IEEE*

***Abstract*—This paper presents a practical strategy for utilizing the submodule (SM) redundancy of a modular multilevel converter (MMC) for its fault tolerance. This strategy provides a systematic framework for balancing the tradeoff between two conventional methods for using the active redundancy and, thus, achieves operational flexibility. One of the existing methods improves SM reliability owing to less voltage stress on the SM components by employing all of the SMs to form the ac or dc voltages (voltage-sharing mode). The other avoids transients by keeping the average SM voltage constant at the cost of slightly increased stress on the SM components (fixed-level mode), which, however, can be controlled to provide the grid-adaptive operation by reserving the energy of the SMs not in service. We, thus, develop a new redundancy management scheme by integrating these two methods and exploiting their technical benefits to meet the PQ requirements and MMC control performance. This research provides a theoretical basis and a technical guide to determining the number of SMs, which can further increase the voltage steps as per the MMC and grid conditions. This paper also connects the remaining PQ capability of the MMC at a particular operating point with the SM redundancy concept by defining a potential redundancy, especially useful when the physical redundancy is exhausted. The theoretical findings and efficacy of the proposed strategy are validated through PSCAD/EMTDC time-domain simulations followed by experiments using a nine-level single-phase MMC system.**

***Index Terms*—Active redundancy, fault tolerance, flexibility, modular multilevel converter (MMC), PQ capability, reliability.**

Manuscript received April 16, 2018; accepted May 29, 2018. Date of publication June 10, 2018; date of current version February 5, 2019. This work was supported in part under the framework of an international cooperation program managed by the National Research Foundation of Korea under Grant 2017K1A4A3013579 and in part by the "Human Resources Program in Energy Technology" of the Korea Institute of Energy Technology Evaluation and Planning, granted financial resource from the Ministry of Trade, Industry & Energy, South Korea, under Grant 20174030201540. Recommended for publication by Associate Editor M. T. Bina. *(Corresponding author: Kyeon Hur.)*

J. Kang, H. Kim, and K. Hur are with the School of Electrical and Electronic Engineering, Yonsei University, Seoul 03722, South Korea (e-mail:

variation may cause some transients and potentially affect the control performance, which is not the case for the first method [23], [24]. Note that the previous research efforts featured their technical benefits independently. This research integrates these conventional active redundancy methods and provides a balanced tradeoff between them according to the MMC internal and external grid conditions. This flexible redundancy scheme offers grid-adaptive flexibility for changing the number of SMs governing the voltage steps. This paper further develops a practical way to access the reserved energy in unused SMs via the conventional redundancy concept. It highlights the enhanced fault tolerance and control performance through the flexible redundancy scheme on the MMC PQ-capability diagram, which informs and illustrates the MMC operating point and its capability effectively. This new perspective helps the system operators gain practical insights into the MMC state and maintain reliable power transfer.

The rest of this paper is organized as follows. Section II gives an overview of the active redundancy methods. Section III details the underlying principle of the flexible redundancy scheme and provides a new perspective on this MMC redundancy by representing its impact on the MMC PQ capability. Section IV demonstrates the validity and efficacy of this research through simulation studies using PSCAD/EMTDC, supported experimentally for the nine-level single-phase MMC as well in Section V. Finally, Section VI provides concluding remarks.

## II. Active Redundancy Method

This section describes two representative active redundancy methods for the MMC. They are the fixed-level and voltage-sharing methods, as addressed in Section I. They are indeed special cases of the proposed flexible redundancy scheme, as illustrated in Fig. 1, where a participation factor $k$ is introduced to quantify the contribution of the SMs among all active redundant SMs to the increase in the number of levels from the nominal value of the fixed-level scheme.

### A. Fixed-Level Method

When the participation factor $k = 0$, the MMC operates in the original fixed-level mode, as shown in Fig. 1(a). The fixed-level method keeps the energy of redundant SMs not participating in the control unused, as shown in Fig. 1(d). There are interesting research efforts for implementing the fixed-level method such as the SM capacitor voltage balancing with pulsewidth modulation (PWM) [11], [21] and nearest level control (NLC) for high-level MMC applications [12], [18], [20]. The redundant SMs do not affect the number of MMC voltage steps; the maximum number of insertion index $n_1(t)$ is $N_s$. The average SM voltage ($\tilde{V}_{C1}$) for the fixed-level method and the electrostatic energy stored in each arm of the converter ($E_{\mathrm{ARM}}$) are, thus, expressed by (1) and (2), respectively, as follows:

$$\tilde{V}_{C1} = \frac{V_C^{\Sigma}}{N_S} \tag{1}$$

$$E_{\mathrm{ARM}} = \frac{1}{2}(N_S + N_R - N_F)C_S\tilde{V}_{C1}^2 \tag{2}$$

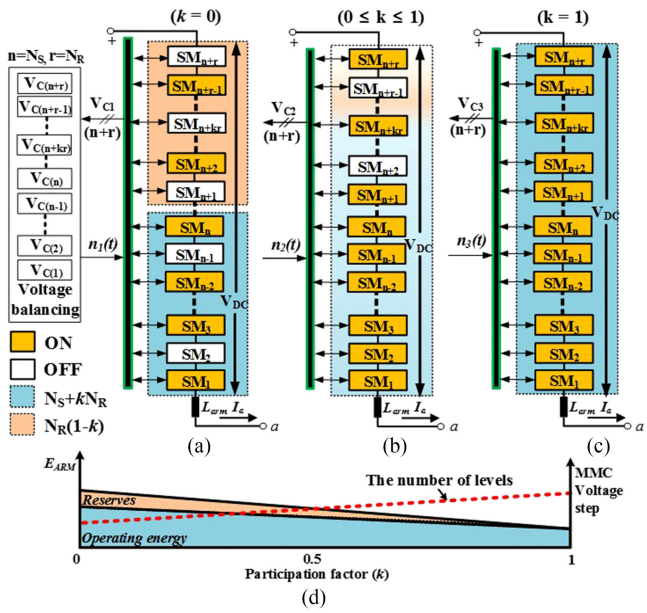


Fig. 1. Principle of redundancy strategy per arm: fixed-level method ($k = 0$), flexible redundancy method ($0 \le k \le 1$) and voltage-sharing method ($k = 1$).

where $N_S$ is the number of SMs for the normal operation of the MMC, $V_C^{\Sigma}$ is the sum of average SM voltage per arm, $N_R$ is the number of redundant SMs, $N_F$ is the number of faulty SMs, and $C_S$ is the capacitance of each individual SM.

The MMC with the fixed-level method continues running with $N_S + 1$ levels with negligible transient in operation because the average SM voltage does not change as long as the $N_F$ does not exceed $N_R$. This method has a positive effect on the capacitor voltage ripple because it employs SMs with higher average voltage (energy) in the switching than the voltage-sharing method, as detailed in the following [21], [22].

### B. Voltage-Sharing Method

In the voltage-sharing method with $k = 1$ [see Fig. 1(c)], the average SM voltage ($\tilde{V}_{C3}$) is less than that of the fixed-level method because all of the redundant SMs account for the voltage steps, which is expressed by (3). The stored energy is also expressed by (4) as follows:

$$\tilde{V}_{C3} = \frac{V_C^{\Sigma}}{N_S + N_R - N_F} \tag{3}$$

$$E_{\mathrm{ARM}} = \frac{1}{2}(N_S + N_R - N_F)C_S\tilde{V}_{C3}^2. \tag{4}$$

All of the SMs in the MMC are utilized to maintain the constant $V_{\mathrm{DC}}$ so that the MMC operates with $N_S + N_R + 1$ levels, i.e., the maximum of $n_3(t)$. This level can be reduced by the number of faulty SMs, and the average SM voltage should then be increased to maintain the desired dc-link voltage through the energy-balancing control [24], [25]. Even with these unavoidable transients, the SM operates at a comparatively low electrostatic energy level, which relieves the stress on the SMs and may increase the overall reliability of the SMs [19].

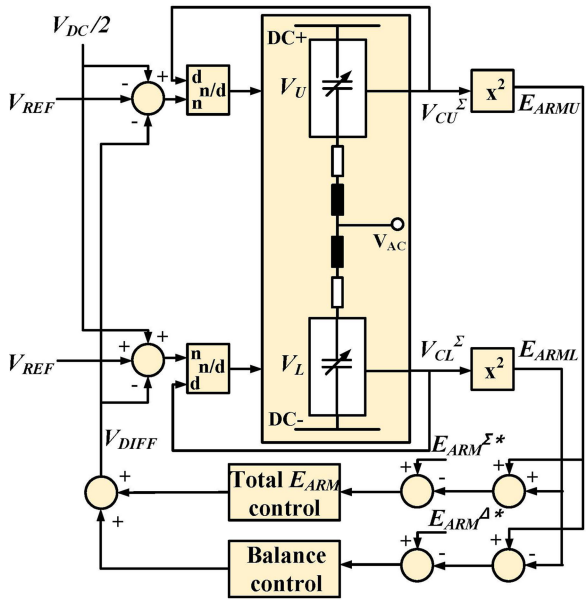


Fig. 2. Arm energy control for flexible redundancy operation.

## III. Flexible Redundancy Strategy

Fig. 1(b) illustrates the principle of the flexible redundancy method. There are numerous technical and economic factors to consider in determining the system parameters such as the SM capacitance $C_S$ for the $(N_S+1)$-level MMC-HVdc applications [26]–[31] and the desired energy–power (EP) ratio of the MMC for various grid requirements, which typically ranges from 10 to 50 kJ/MVA [28]. This paper particularly notes the EP requirement and provides a practical way to implement the flexible redundancy scheme by determining the number of SMs among all of the redundant SMs to further increase the voltage steps. It, thus, relieves the voltage stress by increasing the number of SMs in the fixed-level mode, i.e., by incorporating of the voltage-sharing effect into the fixed-level mode and guaranteeing the desired control performance as well. The energy control adapted from [25] enables the smooth spanning over the two methods (see Fig. 2). Note that this paper focuses on the technical relationship between two existing methods and the benefits of the proposed scheme in operations. The energy storage capability of the $(N_S+1)$-level MMC-HVdc, i.e., $C_S$, and the range of the EP ratio for various operating points are assumed to be determined and given.

### A. Implementation of Flexible Redundancy

The arm capacitance can be related to the EP ratio as follows [28]:

$$C_{\mathrm{ARM}} = \frac{C_S}{N_S} = \mathrm{EP}_0 \frac{S_N}{3V_{\mathrm{DC}}^2} \tag{5}$$

where $C_{\mathrm{ARM}}$ is the total capacitance of the arm, $\mathrm{EP}_0$ is the rated EP ratio, and $S_N$ is the rated power of the MMC. With the redundant SMs in the voltage-sharing mode, the total capacitance of the arm is reduced as follows:

$$C_{\mathrm{ARM}} = \frac{C_S}{N_S+N_R} = \mathrm{EP}_1 \frac{S_N}{3V_{\mathrm{DC}}^2} \tag{6}$$

where $\mathrm{EP}_1$ is the EP ratio with $N_R$. From (5) and (6), $\mathrm{EP}_1$ can be derived as follows:

$$\mathrm{EP}_1 = \frac{N_S}{N_S+N_R}\mathrm{EP}_0. \tag{7}$$

The reduced $\mathrm{EP}_1$ due to $N_R$ should meet the required energy storage capability and the voltage ripple requirements for the feasible operating region, leading to a constraint on the minimum value of $\mathrm{EP}_1$ or $\mathrm{EP}_{\mathrm{MIN}}$

$$\mathrm{EP}_{\mathrm{MIN}} \le \mathrm{EP}_1 = \frac{N_S}{N_S+N_R}\mathrm{EP}_0. \tag{8}$$

From (8), the maximum number of redundant SMs to increase the voltage steps by reinforcing the voltage sharing is determined as

$$N_R \le \frac{N_S}{\mathrm{EP}_{\mathrm{MIN}}}(\mathrm{EP}_0 - \mathrm{EP}_{\mathrm{MIN}}). \tag{9}$$

As an illustrative example, consider an MMC operating with 41 levels ($N_S = 40$), as detailed in Section IV. This paper assumes $\mathrm{EP}_0 = 40$ kJ/MVA and then $\mathrm{EP}_{\mathrm{MIN}} = 30$ kJ/MVA to meet the peak-to-peak voltage ripple (e.g., 10% of the SM capacitor voltage) at a specific operating point, as discussed in [30]–[33]. The maximum allowed redundancy with $N_R = 13$ is then obtained from the EP ratio criterion above and incorporated for fault tolerance. This paper adopts this theoretical maximum redundancy to demonstrate technical implications and benefits of the flexible redundancy scheme, which may be considered unnecessarily high in practice. Fig. 3 compares the SM capacitor voltage ripples as the redundancy scheme and the SM condition change. Based on the effect of active redundancy, as discussed in [21], the capacitor voltage ripple changes in proportion to $(N_S+kN_R)/(N_S+N_R)$ due to the increase in the levels, as demonstrated in Fig. 3. By varying the participation factor $k$, those six redundancy conditions are investigated, and the resulting voltage ripples are compared for three $N_F$ conditions. As understood in [34], the voltage ripple in the voltage-sharing mode ($k=1$) is larger than that in the fixed-level mode ($k=0$) as long as the redundancy, $N_R$, exists. This observation is also confirmed for a test system, as illustrated and summarized in Fig. 3. Compare the percentage of voltage ripples of $k=1$ with those of $k=0$ in Fig. 3(c). Note also the increased SM voltage yet reduced rippled as $N_F$ increases from 0 to 13 (no physical redundancy left when $k=1$). For $k=0$, the average SM voltage does not change, but the ripple increases as $N_F$ grows from 0 to 7. However, the voltage ripples are all less than those when $k=1$ until it exhausts $N_R$ or $N_F = 13$, where the fixed-level and voltage-sharing methods become equivalent for the test system. The benefits of using circulating current suppression control (CCSC) for these conditions are presented as well. The CCSC significantly improves the voltage ripple, as demonstrated in Fig. 3(b) and (d) for the same cases in Fig. 3(a) and (c), which should be considered in the design process.

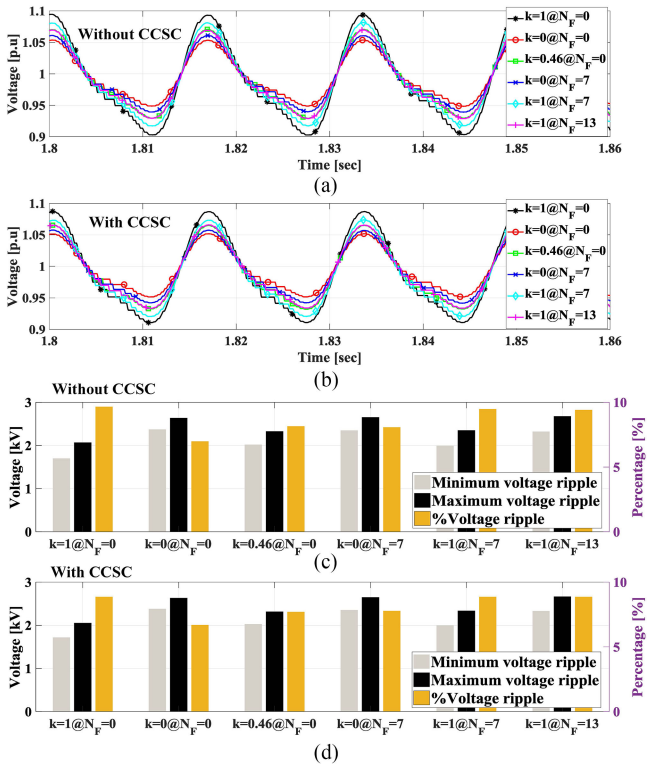


Fig. 3. Comparison of capacitor voltage ripples for three different $N_F$ and $k$ conditions with or without CCSC.

Given the analytical understanding, a participation factor is then determined based on the following reasoning: The flexible redundancy scheme should avoid transients for at least an SM fault by seamlessly bypassing the faulty SM and maintain the voltage ripple less than the marginal performance without any redundancy. It also reserves unused energy for operational flexibility. For example, $k = 0.46@N_F = 0$ is chosen to meet the ripple when $k = 0@N_F = 7$, as shown in Fig. 3(d): their percentages of voltage ripples are close, but the proposed scheme surely reduces the SM voltages. As $k$ increases from 0 toward 1, the voltage-sharing effect is reinforced, and the voltage ripple increases yet. The flexible redundancy scheme aims to provide a balanced tradeoff between these fixed-level and voltage-sharing modes. The electrostatic energy per arm considering the impact of the SM fault is then expressed by (10) as follows:

$$E_{\mathrm{ARM}} = \frac{1}{2}(N_S + N_R - N_F)C_S\left(\frac{V_C^{\Sigma}}{N_S + kN_R - N_F}\right)^2 \tag{10}$$

$$E_{\mathrm{ARM}}^{\Sigma *} = E_{\mathrm{ARMU}} + E_{\mathrm{ARML}}. \tag{11}$$

As shown in Fig. 2, the arm energy controller with the arm energy reference obtained from (11) balances the electrostatic energy of the SM for the SM failure and enables the flexible redundancy scheme. The modulation index ($m$), the reference voltage of the converter ($V_{\mathrm{REF}}(t)$), and the upper ($V_U$) and lower ($V_L$) arm voltages with the flexible redundant SMs can be

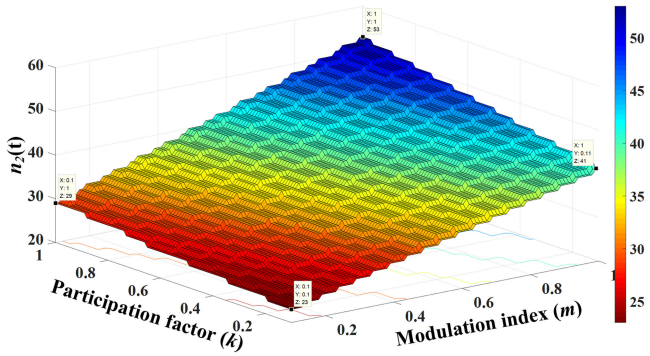


Fig. 4. Insertion indices for various participation factors ($k$) and modulation indices ($m$) for a test system with $N_S = 40$ and $N_R = 13$.

expressed as follows:

$$m = 2\frac{\hat{V}_{\mathrm{AC}}}{V_{\mathrm{DC}}} \tag{12}$$

$$V_{\mathrm{REF}}(t) = \hat{V}_{\mathrm{AC}}\cos(\omega_1 t) = \frac{V_L - V_U}{2} \tag{13}$$

$$V_U = (N_S + kN_R - n_2(t))\left(\frac{V_{\mathrm{DC}}}{N_S + kN_R}\right) \tag{14}$$

$$V_L = n_2(t)\left(\frac{V_{\mathrm{DC}}}{N_S + kN_R}\right) \tag{15}$$

where $n_2(t)$ represents an insertion index (the number of activated SMs) with the flexible redundant SMs. By inserting (14) and (15) into (13), this insertion index can be expressed by (16), which is a function of the participation factor and the modulation index and is associated with $N_S$ and $N_R$, as illustrated in Fig. 4.

$$n_2(t) = \frac{N_S + kN_R}{2}(m\cos(\omega_1 t) + 1). \tag{16}$$

This insertion index can further indicate the number of SMs sharing the voltage yet not being activated in the flexible redundancy scheme. These SMs account for the potential (or soft) redundancy on top of the physical redundancy, $N_R$, as detailed in the following.

### *B. Exploitation of Potential Redundancy*

This research proposes a potential redundancy concept at a certain operating point and quantifies this redundancy in terms of the number of SMs, an equipment operator friendly index for evaluating and exploiting the fault-tolerant capability. Consider a steady-state operating point of the MMC within its PQ capability. Specifically, $\mathrm{MAX}(n_2(t)) \leq N_S + kN_R$ is satisfied because the MMC operates without using all of the SMs [13]. Therefore, the MMC is considered to be operating with extra redundancy, $N_P$

$$N_P = N_S + kN_R - \mathrm{MAX}(n_2(t)). \tag{17}$$

This potential redundancy is a function of $k$ and the insertion index, which depends on the operating point and indicates the operational margin at the operating point.

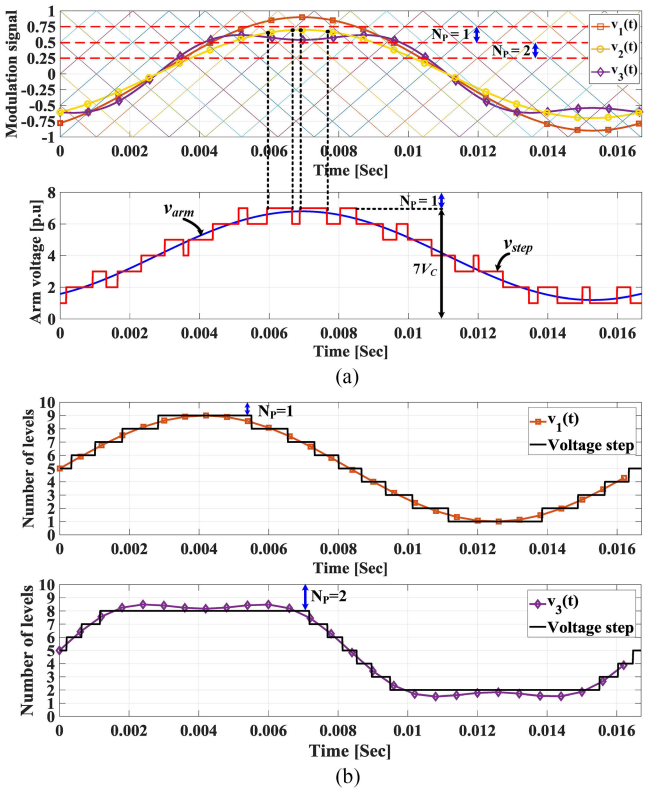


Fig. 5. Principle of potential redundancy without $N_R$ for $v_1(t) = 0.8\sin(\omega_1 t)$, $v_2(t) = 0.7\sin(\omega_1 t)$, and $v_3(t) = 0.8\sin(\omega_1 t) + 0.16\sin(3\omega_1 t)$. (a) PSC-PWM with $N_s = 8$. (b) NLC with $N_s = 10$.

*1) Potential Redundancy With PWM:* Fig. 5(a) illustrates the underlying concept of the potential redundancy for an MMC with a phase-shifted carrier-based PWM (PSC-PWM). As an illustrative example, the MMC runs out of the physical redundancy. Compare the peak value of the modulating signal ($v_2(t)$) with cross points of the phase-shifted carriers, which is in the range between 0.5 and 0.75. The signal $v_1(t)$ is over this range so that there is no potential redundancy in the MMC. The $v_2(t)$, however, runs with the potential redundancy because the MMC does not operate with all of the SMs. By inserting (16) into (17), $N_P$ can be calculated for this case as

$$N_P = (N_S + kN_R)\left(1 - \frac{1}{2}(m+1)\right). \tag{18}$$

Because $N_P$ is defined to be an integer, it should further be rounded to the next smaller integer by the floor$\{\}$ function, as shown in (19a). As $v_3(t)$ is from $v_1(t)$ with the third harmonic injection [35], the number of redundant SMs ($N_{P3}$) can be calculated by (19b) [see Fig. 5(a)] as

$$N_P = \text{floor}\left\{(N_S + kN_R)\left(1 - \frac{1}{2}(m+1)\right)\right\} \tag{19a}$$

$$N_{P3} = \text{floor}\left\{(N_S + kN_R)\left(1 - \frac{1}{2}\left(\frac{\sqrt{3}}{2}m + 1\right)\right)\right\}. \tag{19b}$$

*2) Potential Redundancy With NLC:* The number of activated SMs can be derived from the relationship with the modulation signal as follows:

$$n_2(t) = \text{round}\left\{\frac{N_S + kN_R}{2}\left(m\cos(\omega_1 t) + 1\right)\right\}. \tag{20}$$

The potential redundancy with the NLC switching is then calculated by finding the nearest integer via the round$\{\}$ function, as shown in Fig. 5(b). From (17) and (20), the potential redundancy can be expressed by (21a). The result of applying the third harmonic injection leads to (21b), which confirms that more redundancy can be secured, as shown in Fig. 5(b)

$$N_P = N_S + kN_R - \text{round}\left\{\frac{N_S + kN_R}{2}(m+1)\right\} \tag{21a}$$

$$N_{P3} = N_S + kN_R - \text{round}\left\{\frac{N_S + kN_R}{2}\left(\frac{\sqrt{3}}{2}m + 1\right)\right\}. \tag{21b}$$

TABLE I
SYSTEM PARAMETERS OF THE SIMULATION

| Parameters | Value |
|---|---|
| Rated active power $P_{dc}$ (MW) | 100 |
| DC-link voltage $V_{dc}$ (kV) | $\pm$ 50 |
| Line inductance $L_s$ (mH) | 1.0 |
| Short circuit ratio $SCR$ | 8.64 |
| Number of normal SMs per arm | 40 |
| Number of redundant SMs per arm | 13 |
| Nominal SM capacitance $C_s$ ($\mu$F) | 5330 |
| Arm inductance $L_{arm}$ (mH) | 50 |
| Nominal capacitor voltage $V_c$ ($kV$) | 2.5 |
| Energy-power ratio $EP_0$ (kJ/MVA) | 40 |
| Participation factor $k$ | 0.46 |

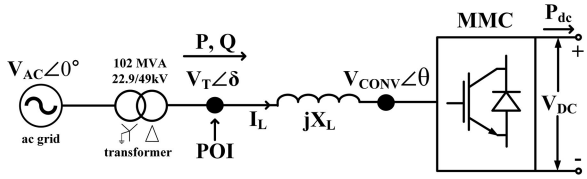


Fig. 6. Simple MMC-HVdc model.

*3) Potential Redundancy in the MMC PQ Capability:* Table I shows the system parameters for determining the potentially redundant SMs with the flexible redundancy scheme to contribute to the MMC fault tolerance of a simple system depicted in Fig. 6, which shows that the MMC-HVdc system absorbs real power in the rectifier mode with reactive power transfer for unity-power-factor operation on the point of interconnection (POI). The potential redundancy of the MMC-HVdc is associated with the remaining capability in the PQ region at a specific operating point, as illustrated in Fig. 6: the MMC has 40 SMs per arm with 13 redundant SMs and operates at $p_1$ in the steady state. At this point, for the available power transfer, as indicated in Table I, the modulation index ($m$) is approximately 0.8, which is calculated by (22) through the value obtained from a relation between the PQ capability and the vector diagram in

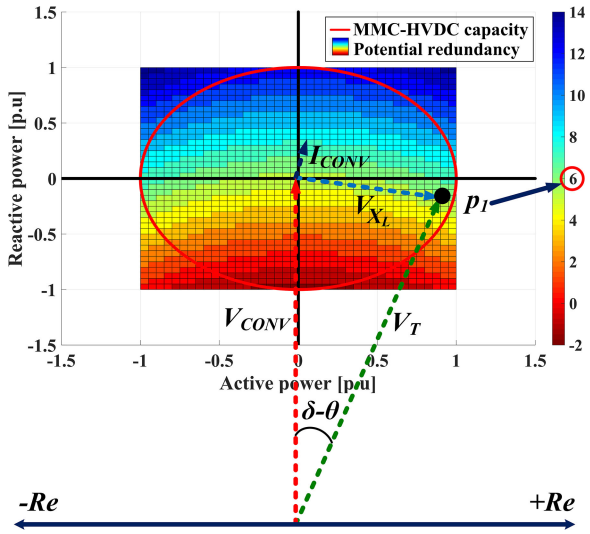


Fig. 7. Potential redundancy capability in the PQ-capability diagram of the rectifier mode of MMC-HVdc with reactive power for unity power factor on the POI: point $p_1$ indicates the number of potential redundant SMs within the PQ region.

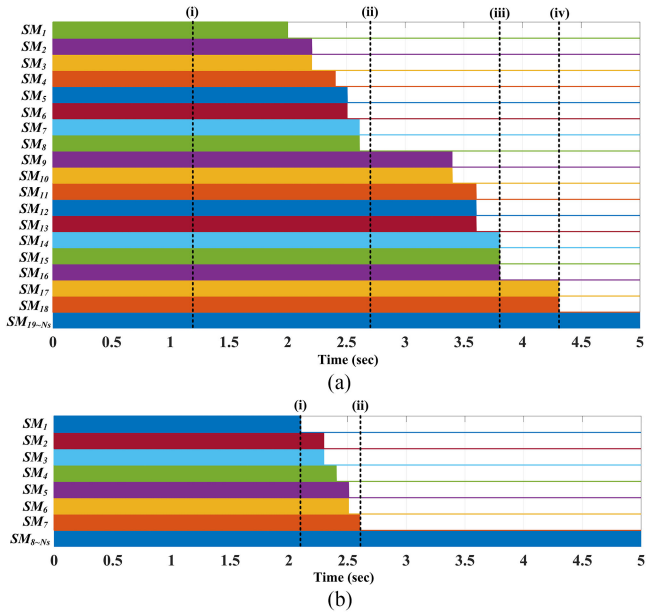


Fig. 8. (a) Upper and (b) lower switching states for the test scenario.

Fig. 7 as follows:

$$m = 2\frac{V_{\mathrm{CONV}}}{V_{\mathrm{DC}}}\sqrt{\frac{2}{3}}. \tag{22}$$

As a result, the number of potentially redundant SMs is 6, which is calculated by (19b) with $k = 0$, and this MMC system is, thus, equipped with 19 redundant SMs: six SMs (potential redundancy) on top of 13 SMs. Therefore, the redundant SMs provide the MMC with strong fault-tolerant capability, which is validated through time-domain simulations in Section IV. This potential redundancy surely depends on the operating point (modulation index and power angle). As shown in Fig. 7, the number of potentially redundant SMs increases as the reactive power decreases and further provides it back to the grid. As the modulation index determines the converter ac voltage, which is coupled with the required reactive power in the grid connected to the MMC, the potential redundancy is associated with the reactive power compensation. Thus, there is a tradeoff between a fault tolerance and the reactive power compensation for the grid. In addition, the converter voltage limit with respect to a grid condition is a critical factor for the potential redundancy capability in the PQ-capability region.

## IV. Simulation Results

In order to demonstrate the fault-tolerant operation of the MMC with the flexible redundancy scheme, simulations are conducted using PSCAD/EMTDC with the system parameters listed in Table I. Energy control for the MMC is implemented with the proposed redundancy strategy, as shown earlier in Fig. 2. Fig. 8 illustrates the switching states of the SMs of the test system for an operating scenario: Colored bars indicate that those corresponding SMs run until the bars ends. The vertical line (i) in Fig. 8(a) indicates that the flexible redundancy mode is activated after the full voltage-sharing method. The maximum

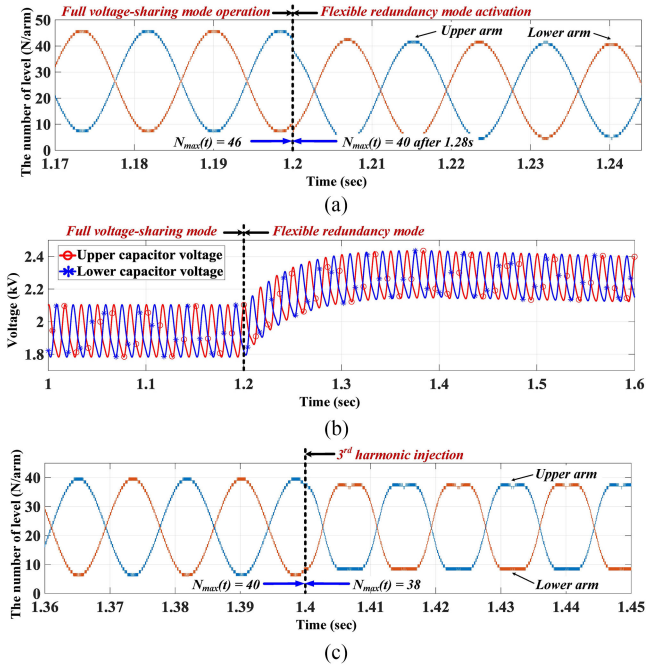


Fig. 9. (a) Number of activated SMs and (b) capacitor voltages after flexible redundancy activation. (c) Number of activated SMs after injecting third harmonic reference.

number of activated SMs is then reduced from 46 to 40, as shown in Fig. 9(a). Thus, six redundant SMs reduce the voltage-sharing effect (from $k = 1$ to $k = 0.46$) and contribute to the increase of the average SM voltage. The number of redundant SMs in the fixed-level mode (not contributing to the increase of the MMC levels) is still seven. Note that the average capacitor voltage increases, as shown in Fig. 9(b). The third harmonic is injected in the modulation signal to further reduce the insertion indices, as shown in Fig. 9(c). Line (ii) in Fig. 8(a) indicates that the

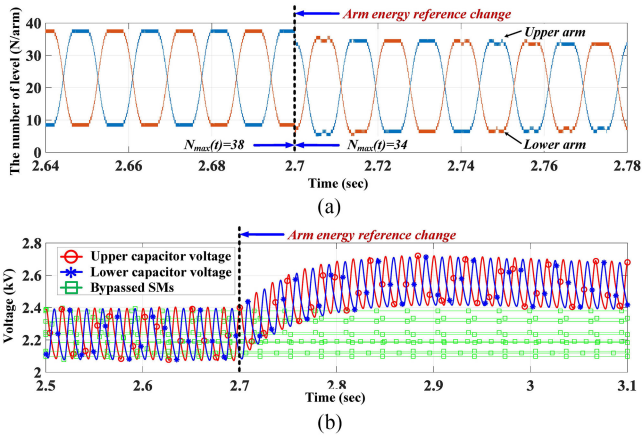


Fig. 10. (a) Number of activated SMs and (b) capacitor voltages in the case of arm reference change.

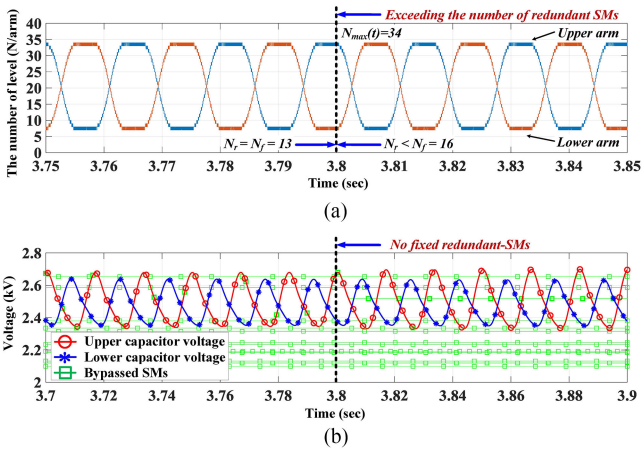


Fig. 11. (a) Number of activated SMs and (b) capacitor voltages in the case the number of faulty SMs exceeds the number of redundant SMs.

arm energy reference is changed after the redundant SMs in the fixed-level mode are exhausted. The maximum number of activated SMs in real time decreases from 38 to 34, as shown in Fig. 10(a). Consequently, the average capacitor voltage increases and is able to maintain the nominal capacitor voltage rating (2.5 kV), as shown in Fig. 10(b). It indicates that the potentially redundant SMs at the operating point within the PQ capability are capable of providing the additional fault tolerance to the MMC system with the faulty SMs not replaced yet. As shown in Fig. 8(b), this research further considers a situation where additional SM fault occurs only in the upper arm. Even though the potential redundancy provides the MMC with the fault tolerance without any physically redundant SMs, this unbalanced condition increases the capacitor voltage ripple in the upper arm, as observed in Figs. 11 and 12. The increased capacitor voltage ripple results in the fundamental component (60 Hz) in the circulating current, which, however, can be eliminated by the unbalanced arm energy control [36]–[39].

## V. Experimental Results

Fig. 13 shows the experimental setup for the nine-level single-phase MMC with eight SMs per arm, i.e., 16 SMs in total.

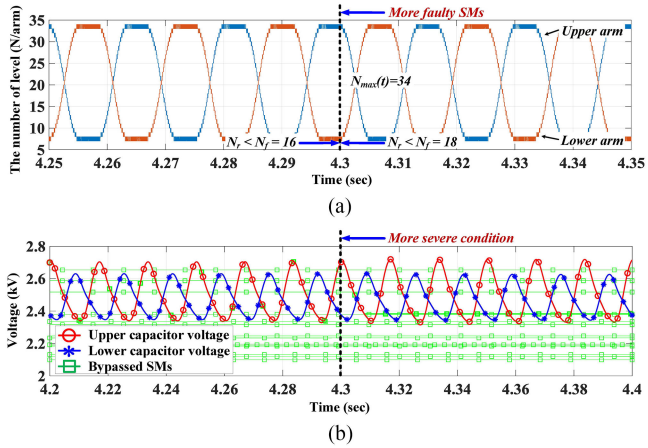


Fig. 12. (a) Number of activated SMs and (b) capacitor voltages in a more severe faulty condition.

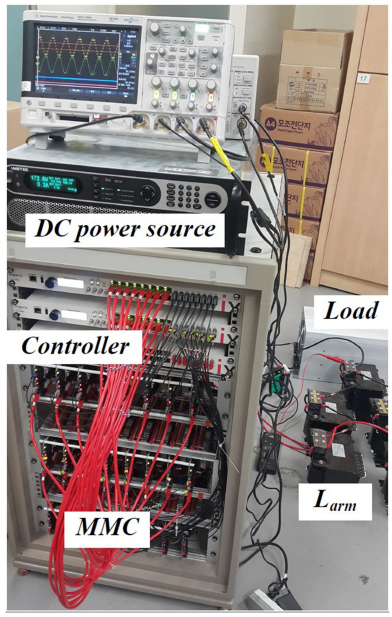


Fig. 13. Photograph of the experimental setup.

The system specification is as follows: $C_S = 1815\ \mu$F, $L_{\text{arm}} = 10$ mH, $L_{\text{load}} = 5$ mH, $R_{\text{load}} = 50\ \Omega$, $V_{\text{dc}} = 300$ V, and an bypass switch for the assumed SM failure. The upper arm includes $\text{SM}_1$–$\text{SM}_8$ and the lower arm includes $\text{SM}_9$–$\text{SM}_{16}$. As discussed earlier in Section II and shown in Fig. 14(a), the voltage sharing method ($k = 1$) affects the capacitor voltage, the arm voltage, and the number of levels in the MMC when the $\text{SM}_2$ fault occurs. It also causes the unbalanced condition in the MMC, as observed in Fig. 14(b). To demonstrate the effectiveness of the flexible redundancy method, the number of levels of the MMC originally with nine levels in the full voltage-sharing mode is reduced to $n_2(t) = 7$ with $k = 0.5$ (see Fig. 15). Under this condition, the SM voltage ripple ($\Delta V_{C1}$) is reduced to $\Delta V_{C1}^{'}$. There is no impact on the SM voltages and the number of levels for an SM fault due to the active redundancy in the

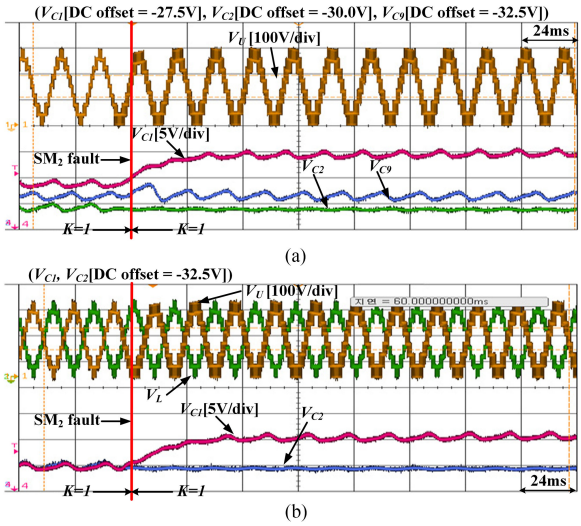


Fig. 14. Arm and capacitor voltages of the MMC with redundancy in the voltage-sharing method for an SM fault. (a) Upper arm voltage and capacitor voltages. (b) Upper and lower arm voltages and capacitor voltages.

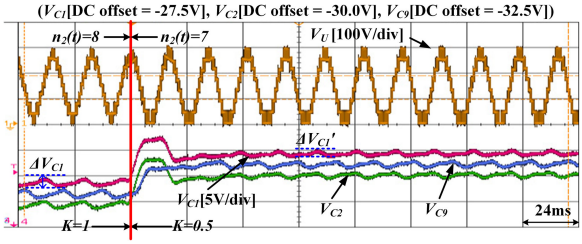


Fig. 15. Reduced capacitor voltage ripple by changing the arm reference in the flexible redundancy.

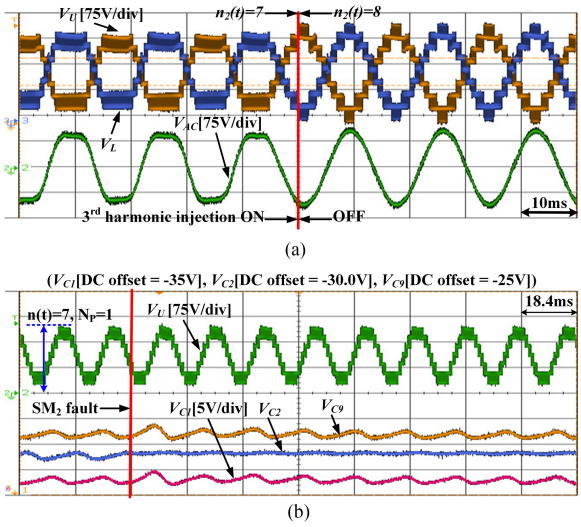


Fig. 16. Potential redundancy via the third harmonic injection. (a) Upper and lower arm voltages and ac voltage with and without the third harmonic injection. (b) Upper arm and capacitor voltages for an SM fault.

fixed-level mode, which is not shown in this paper, though (see further discussion in [11] and [21]).

The number of activated SMs with the third harmonic injection is also presented in Fig. 16(a). This experiment is designed to demonstrate that the flexible redundancy may enhance the fault-tolerant operation of the MMC system at the specified operating point by evaluating the potential redundancy, as shown in Fig. 16(b).

## VI. Conclusion

This research has investigated the use of redundant SMs of the MMC. Device reliability (due to voltage stress on the SM components) and transient control performance (due to the SM voltage change for the SM fault) are the primary factors for consideration. Those extra SMs may participate in forming the ac and dc waveforms or remain energized until an SM fault occurs depending on the conventional strategies in a deterministic way. The proposed strategy connects these methods and adds to flexibility in order to manage the SM voltage stress, ripples, and transients for the SM fault. Specifically, this flexibility allows for using the energy stored in some redundant SMs not participating in the MMC control and may enable the grid service such as inertial response in emergency. This opportunity may become more valuable owing to continuously increasing variable renewable generation. It is also worth noting that this paper sheds new light on the MMC PQ capability associated with the SM redundancy, considered to be crucial to making the most of the MMC. This new perspective may refine the current redundancy design process. The technical guide should be a useful reference for determining and managing the SM redundancy of the MMC and for planning the MMC operations adaptive to the dynamically changing grid conditions.

## References

[1] A. Lesnicar and R. Marquardt, "An innovative modular multilevel converter topology suitable for a wide power range," in *Proc. IEEE Bologna Power Tech Conf.*, Jun. 2003, pp. 1–6.

[2] N. Flourentzou, V. G. Agelidis, and G. D. Demetriades, "VSC-based HVDC power transmission systems: An overview," *IEEE Trans. Power Electron.*, vol. 24, no. 3, pp. 592–602, Mar. 2009.

[3] M. Hagiwara and H. Akagi, "Control and experiment of pulsewidth-modulated modular multilevel converters," *IEEE Trans. Power Electron.*, vol. 24, no. 7, pp. 1737–1746, Jul. 2009.

[4] S. Debnath, J. Qin, B. Bahrani, M. Saeedifard, and P. Barbosa, "Operation, control, and applications of the modular multilevel converter: A review," *IEEE Trans. Power Electron.*, vol. 30, no. 1, pp. 37–53, Jan. 2015.

[5] H. Kim, S. Kim, Y.-H. Chung, D.-W. Yoo, C.-K. Kim, and K. Hur, "Operating region of modular multilevel converter for HVDC with controlled second-order harmonic circulating current: elaborating P-Q capability," *IEEE Trans. Power Del.*, vol. 31, no. 2, pp. 493–502, Apr. 2016.

[6] H. Liu, C. Loh, and F. Blaabjerg, "Review of fault diagnosis and fault-tolerant control for modular multilevel converter of HVDC," in *Proc. 39th Annu. Conf. IEEE Ind. Electron. Soc.*, Nov. 2013, pp. 1242–1247.

[7] C. L. Tho and L. E. Norum, "Implementation of high speed control network with fail-safe control and communication cable redundancy in modular multilevel converter," in *Proc. 15th Eur. Conf. Electron. Appl.*, Sep. 2013, pp. 1–10.

[8] R. Teodorescu, E.-P. Eni, L. Mathe, and P. Rodriguez, "Modular multilevel converter control strategy with fault tolerance," in *Proc. Int. Conf. Renew. Energies Power Qual.*, 2013, pp. 1–6.

[9] P. D. Burlacu, L. Mathe, M. Rejas, H. Pereira, A. Sangwongwanich, and R. Teodorescu, "Implementation of fault tolerant control for modular multilevel converter using EtherCAT communication," in *Proc. IEEE Int. Conf. Ind. Technol.*, Mar. 2015, pp. 3064–3071.

[10] R. Picas, J. Zaragoza, J. Pou, and S. Ceballos, "Reliable modular multilevel converter fault detection with redundant voltage sensor," *IEEE Trans. Power Electron.*, vol. 32, no. 1, pp. 39–51, Jan. 2017.

[11] J.-Y. Choi and B.-M. Han, "An improved phase-shifted carrier PWM for modular multilevel converters with redundancy sub-modules," *J. Power Electron.*, vol. 16, no. 2, pp. 473–479, Mar. 2016.

[12] H. Saad, X. Guillaud, J. Mahseredjian, S. Dennetière, and S. Nguefeu, "MMC capacitor voltage decoupling and balancing controls," *IEEE Trans. Power Del.*, vol. 30, no. 2, pp. 704–712, Apr. 2015.
[13] G. Liu, Z. Xu, Y. Xue, and G. Tang, "Optimized control strategy based on dynamic redundancy for the modular multilevel converter," *IEEE Trans. Power Electron.*, vol. 30, no. 1, pp. 339–348, Jan. 2015.
[14] Q. Yang, J. Qin, and M. Saeedifard, "A post-fault strategy to control the modular multilevel converter under submodule failure," *IEEE Trans. Power Del.*, vol. 31, no. 6, pp. 2453–2463, Dec. 2016.
[15] L.-A. Grégoire, H. F. Blanchette, W. Li, A. Antonopoulos, L. Ängquist, and K. Al-Haddad, "Modular multilevel converter overvoltage diagnosis and remedial strategy during blocking sequence," *IEEE Trans. Power Electron.*, vol. 30, no. 5, pp. 2777–2785, May 2015.
[16] B. Gemmell, J. Dorn, D. Retzmann, and D. Soerangr, "Prospects of multilevel VSC technologies for power transmission," in *Proc. Transmiss. Distrib. Conf. Expo.*, May 2008, pp. 1–16.
[17] B. Li, Y. Zhang, R. Yang, R. Xu, D. Xu, and W. Wang, "Seamless transition control for modular multilevel converters when inserting a cold-reserve redundant submodule," *IEEE Trans. Power Electron.*, vol. 30, no. 8, pp. 4052–4057, Aug. 2015.
[18] P. Hu, D. Jiang, Y. Zhou, Y. Liang, J. Guo, and Z. Lin, "Energy-balancing control strategy for modular multilevel converters under submodule fault conditions," *IEEE Trans Power Electron.*, vol. 29, no. 9, pp. 5021–5030, Sep. 2014.
[19] J. Guo, X. Wang, J. Liang, H. Pang, and J. Gonçalves, "Reliability modeling and evaluation of MMCs under different redundant schemes," *IEEE Trans. Power Del.*, accepted for publication.
[20] G. T. Son *et al.*, "Design and control of a modular multilevel HVDC converter with redundant power modules for noninterruptible energy transfer," *IEEE Trans. Power Del.*, vol. 27, no. 3, pp. 1611–1619, Jul. 2012.
[21] G. Konstantinou, J. Pou, S. Ceballos, and V. G. Agelidis, "Active redundant submodule configuartion in modular multilevel converters," *IEEE Trans. Power Del.*, vol. 28, no. 4, pp. 2333–2341, Oct. 2013.
[22] G. S. Konstantinou, M. Ciobotaru, and V. G. Agelidis, "Effect of redundant sub-module utilization on modular multilevel converters," in *Proc. IEEE Int. Conf. Ind. Technol.*, Mar. 2012, pp. 815–820.
[23] K. Sharifabadi, L. Harnefors, H.-P. Nee, S. Norrga, and R. Teodorescu, *Design, Control, and Application of Modular Multilevel Converters for HVDC Transmission System*. West Sussex, U.K.: Wiley–IEEE Press, 2016, pp. 60–127.
[24] N. Ahmed, L. Ängquist, A. Antonopoulos, L. Harnefors, S. Norrga, and H.-P. Nee, "Performance of the modular multilevel converter with redundant submodules," in *Proc. 41th Annu. Conf. IEEE Ind. Electron. Soc.*, Nov. 2015, pp. 3922–3927.
[25] A. Antonopoulos, L. Ängquist, and H.-P. Nee, "On dynamics and voltage control of the modular multilevel converter," in *Proc. Eur. Conf. Power Electron. Appl.*, Barcelona Spain, 2009, pp. 1–10.
[26] G. Ding, M. Ding, and G. Tang, "An innovative modular multilevel converter topology and modulation control scheme for the first VSC-HVDC project in China," in *Proc. 37th Annu. Conf. IEEE Ind. Electron. Soc.*, Jan. 2011.
[27] M. M. C. Merlin and T. C. Green, "Cell capacitor sizing in multilevel converters: Cases of the modular multilevel converter and alternate arm converter," *IET Power Electron.*, vol. 8, no. 3, pp. 350–360, Mar. 2015.
[28] M. Zygmanowski, B. Grzesik, and R. Nalepa, "Capacitance and inductance selection of the modular multilevel converter," in *Proc. 15th Eur. Conf. Power Electron. Appl.*, Sep. 2015, pp. 1–10.
[29] M. Eremia, C.-C. Liu, and A.-A. Edris, *Advanced Solution in Power Systems: HVDC, FACTS, and Artificial Intelligence*. Piscataway, NJ, USA: Wiley–IEEE Press, Oct. 2016, pp. 144–147.
[30] B. Jacobson, P. Karlsson, G. Asplund, L. Harnefors, and T. Jonsson, "VSC-HVDC transmission with cascaded two-level converters," in *Proc. CIGRE Session*, 2010, Paper B4-110.
[31] K. Ilves, S. Norrga, L. Harnefors, and H.-P. Nee, "On energy storage requirements in modular multilevel converters," *IEEE Trans. Power Electron.*, vol. 29, no. 1, pp. 77–88, Jan. 2014.
[32] A. Beddard and M. Barnes, "Modelling of MMC-HVDC systems—An overview," *Energy Procedia*, vol. 80, pp. 201–212, Dec. 2015.
[33] Y. Li, X. Shi, B. Liu, F. Wang, and W. Lei, "Maximum modulation index for modular multilevel converter with circulating current control," in *Proc. IEEE Energy Convers. Congr. Expo.*, Sep. 2014, pp. 491–498.
[34] C. Oates, "Modular multilevel converter design for VSC HVDC application," *IEEE Trans. Power Electron.*, vol. 3, no. 2, pp. 505–515, Jun. 2015.
[35] J. A. Houldsworth and D. A. Grant, "The use of harmonic distortion to increase the output voltage of a three-phase PWM inverter," *IEEE Trans. Ind. Appl.*, vol. IA-20, no. 5, pp. 1224–1228, Sep./Oct. 1984.
[36] F. Deng, Y. Tian, R. Zhu, and Z. Chen, "Fault-tolerant approach for modular multilevel converters under submodule faults," *IEEE Trans. Ind. Electron.*, vol. 63, no. 11, pp. 7253–7263, Nov. 2016.
[37] W. Wu, X. Wu, J. Yin, L. Jing, S. Wang, and J. Li, "Characteristic analysis and fault-tolerant control of circulating current for modular multilevel converters under sub-module faults," *Energies*, vol. 26, no. 7, pp. 1444–1461, Nov. 2017.
[38] Z. Wang, A. Zhang, H. Zhang, and Z. Ren, "Control strategy for modular multilevel converters with redundant sub-modules using energy reallocation," *IEEE Trans. Power Del.*, vol. 32, no. 3, pp. 1556–1564, Jun. 2017.
[39] J. Kang, H. Kim, H.-J. Jung, D.-S. Lee, and K. Hur, "Fault-tolerant operation scheme for modular multilevel converter under arm energy imbalance," in *Proc. IEEE 12th Int. Conf. Power Electron. Drive Syst.*, Dec. 2017, pp. 6628–6637.

**Jaesik Kang** (S'11–M'13) received the M.Sc. degree in electrical and electronic engineering in 2013 from Yonsei University, Seoul, South Korea, where he is currently working toward the Ph.D. degree in electrical and electronic engineering.

He was a Research and Development Engineer with the Korea Railroad Research Institute, Uiwan, South Korea, in 2013. He was with LG Display, Paju, South Korea, between 2013 and 2014. His research interests include modeling and control of power converters, modular multilevel converters, flexible ac transmission systems/high-voltage direct current, and power electronic applications in power systems.

**Heejin Kim** (S'10–M'15) received the B.S. and Ph.D. degrees in electrical engineering from the School of Electrical and Electronic Engineering, Yonsei University, Seoul, South Korea, in 2010 and 2015, respectively.

He is currently a Postdoctoral Fellow with Yonsei University. His research interests include modeling and control of power converters, modular multilevel converters, flexible ac transmission systems/high-voltage direct current, and power electronic applications in power systems.

**Hong-Ju Jung** (S'98–M'00–SM'15) received the B.S. and M.S. degrees in electrical engineering from Kwangwoon University, Seoul, South Korea, in 1998 and 2000, respectively, and the Ph.D. degree from Hanyang University, Seoul, in 2015.

Since 2000, he has been with Hyosung Corporation, where he is currently Chief Researcher with the Hyosung Power and Industrial Systems R&D Center, Anyang, South Korea. His main research interests include power converter systems for renewable energies and high-voltage direct current/flexible ac transmission system converter systems.

**Dong-Su Lee** (S'04–M'06) received the B.S. and M.S. degrees in electrical engineering from Hongik University, Seoul, South Korea, in 2004 and 2006, respectively.

Since 2007, he has been with Hyosung Corporation, where he is currently Senior Researcher at the Hyosung Power and Industrial Systems R&D Center, Anyang, South Korea. He has worked on geographical information system (GIS) development research from 2007 to 2009 and has experience in reliability evaluation of GIS and high-voltage electric motors from 2010 to 2014. From 2014 to 2017, he worked in the Power Systems Study Group and currently works for the HVdc Development Team.

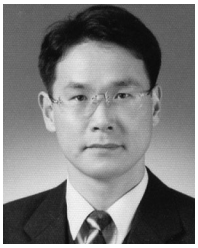

**Chan-Ki Kim** (M'95–SM'05) received the M.Sc. and Ph.D. degrees in electrical engineering from Chung-Ang University, Seoul, South Korea, in 1993 and 1996, respectively.

Since 1996, he has been with Korea Electric Power Research Institute, the R&D center of Korea Electric Power Corporation, Daejeon, South Korea. He has authored or coauthored more than 46 technical papers in widely read journals, including Korean Institute of Electrical Engineers (KIEE) journals and IEEE transactions, and submitted 40 patents and programs and has published an HVdc book entitled *HVDC Transmission—Power Conversion Application in Power System* (New York, NY, USA: Wiley–IEEE Press, 2009). He developed the HVdc simulator, HVdc commissioning technology, and HVdc control algorithms. His research interests include HVdc and power electronics.

Dr. Kim was a recipient of the Technical Award from the Ministry of Science and Technology of the Korean Government and Excellent Paper Awards from the KIEE in 2002, 2004, and 2014. He is a senior member of the KIEE.

**H. Alan Mantooth** (S'83–M'90–SM'97–F'09) received the B.S. *(summa cum laude)* and M.S. degrees in electrical engineering from the University of Arkansas, Fayetteville, AR, USA, in 1985 and 1986, respectively, and the Ph.D. degree from the Georgia Institute of Technology, Atlanta, GA, USA, in 1990.

In 1990, he joined Analogy, where he focused on semiconductor device modeling and the research and development of hardware-description-language-based modeling tools and techniques. Besides modeling, his interests include analog and mixed-signal integrated circuit (IC) design and power electronics. In 1998, he joined the faculty of the Department of Electrical Engineering, University of Arkansas, where he has been a Full Professor with the Department of Electrical Engineering since 2002. In 2003, he co-founded Lynguent, an EDA company focused on modeling and simulation tools. He established the National Center for Reliable Electric Power Transmission (NCREPT), University of Arkansas, in 2005. In 2006, he was the inaugural holder of the 21st Century Endowed Chair in Mixed-Signal IC Design and CAD. He has authored or coauthored more than 200 refereed articles on modeling and IC design. He holds patents on software architecture and algorithms for modeling tools and has others pending. He has coauthored three books and has served on several technical program committees for IEEE conferences.

Dr. Mantooth is the President of the IEEE Power Electronics Society. He is a member of Tau Beta Pi and Eta Kappa Nu, and registered Professional Engineer in Arkansas. He is the Executive Director for NCREPT and GRid-connected Advanced Power Electronic Systems (GRAPES) as well as two of its constitutive centers of excellence: the National Science Foundation (NSF) Industry/University Cooperative Research Center on GRAPES and the NSF Established Program to Stimulate Competitive Research (EPSCoR) Vertically Integrated Center on Transformative Energy Research. He is also the Director of the NSF EPSCoR GREEN Center for Nanoplasmonic Solar Cell Research.

**Kyeon Hur** (S'04–M'07–SM'12) received the B.S. and M.S. degrees in electrical engineering from Yonsei University, Seoul, South Korea, in 1996 and 1998, respectively, and the Ph.D. degree in electrical and computer engineering from the University of Texas at Austin, TX, USA, in 2007.

Between 1998 and 2003, he was an R&D Engineer with Samsung Electronics, Suwon, South Korea, where he designed control algorithms and power-electronic circuits for ac drives. Between 2007 and 2008, he was a Grid Operations Engineer with the Electric Reliability Council of Texas, Taylor, TX, where he supported real-time grid operations by conducting power flow and stability analyses and managing state estimators. From 2008 to 2010, he was with the Electric Power Research Institute, Palo Alto, CA, USA, and conducted and managed research projects in Grid Operations and Planning, regarding phasor measurement unit (PMU)-based protection and control, reactive power management and control, and flexible ac transmission systems/high-voltage direct current (FACTS/HVDC). Since 2010, he has been with Yonsei University, where he leads a smart-grid research group. His current research interests include FACTS/HVDC, PMU-based analysis and control, integration of variable generation and controllable load, and load modeling.

Dr. Hur is an Associate Editor for the *Journal of Power Electronics* and the *Journal of Electrical Engineering and Technology*.